ELSEVIER

A framework for numerical integration of crystal elasto-plastic constitutive equations compatible with explicit finite element codes

Alireza V. Amirkhizi, Sia Nemat-Nasser *

Deparmtment of Mechanical and Aerospace Engineering, Center of Excellence for Advanced Materials, University of California, San Diego, 4209 Engineering Building 1, 9500 Gilman Drive, La Jolla, CA 92093-0416, United States

Abstract

In this paper we summarize the elements of a numerical integration scheme for elasto-plastic response of single crystals. This is intended to be compatible with large-scale explicit finite element codes and therefore can be used for problems involving multiple crystals and also overall behavior of polycrystalline materials. The steps described here are general for anisotropic elastic and plastic response of crystals. The crystallographic axes of the lattice are explicitly stored and updated at each time step. A plastic predictor–elastic corrector scheme is used to calculate the plastic strain rates on all active slip systems based on a rate-dependent physics-based constitutive model without the need of further auxiliary assumptions. Finally we present the results of numerous calculations using a physics-based rate- and temperature-dependent model of copper and the effect of elastic unloading, elastic crystal anisotropy, and deformation-induced lattice rotation are emphasized.
© 2007 Elsevier Ltd. All rights reserved.

Keywords: Physics-based modeling; Crystal plasticity; Elastoplastic anisotropy; Numerical algorithm

1. Introduction

Taylor (1934), Orowan (1934) and Polanyi (1934) independently but at the same time showed that the plastic deformation of crystalline metals is due to the dislocation-induced

---

* Corresponding author. Tel.: +1 858 534 4914; fax: +1 858 534 2727.
  E-mail address: sia@ucsd.edu (S. Nemat-Nasser).

slip on preferred crystallographic planes and in preferred directions. Based on this physical understanding, one can in principal model the deformation of a single crystal under prescribed loads or calculate the forces required to induce a given deformation. However, the number of possible slip systems is usually more than 5, which is the number of independent variables in a general deviatoric deformation tensor increment, and therefore the problem is under-determined. Bishop and Hill (1951a,b) partly overcame this difficulty by using the principle of maximum plastic work. Lin (1957) and Lin and Ito (1966) emphasized the effect of elasticity and also showed that, in fact, various slip systems can become active sequentially as the deformation progresses. Peirce et al. (1983) and Nemat-Nasser and Obata (1986) used an explicit scheme to calculate and integrate the slip rates on all slip systems. Finally Nemat-Nasser and Okinaka (1996) used a plastic predictor–elastic corrector algorithm for the integration that converges for much greater time-steps than those required in forward-gradient methods. For a thorough look at various aspects of crystal plasticity see Havner (1994) and Nemat-Nasser (2004, Chapter 6).

These contributions and much of the other recent research (see Kaldindini et al., 1992; Cuitiño and Ortiz, 1992; Bronkhorst et al., 1992; Beaudoin et al., 1993; Bate, 1999 and Kuchnicki et al., 2006) are usually aimed at the prediction of the overall properties of polycrystalline metals and therefore employ some homogenization technique, most notably Taylor averaging, or ad hoc arrangement of the single crystals. Furthermore they mainly rely on power-law constitutive relations. Most recently McGinty and McDowell (2006) discuss their work in relation to an earlier work by Nemat-Nasser et al. (1998b) where the plastic predictor–elastic corrector method of Nemat-Nasser and co-workers (see Nemat-Nasser (2004, Chapter 5), for detail discussion and references) have been applied to bcc and fcc crystals. In addition, they do make contact with the yet earlier work of Rashid and Nemat-Nasser (1992) that uses the plastic predictor with iteration and shows that one or two iterations give excellent results. They also point out the substantial difference between the plastic predictor method and the classical elastic predictor method, with the latter having been used by, among others, Cuitiño and Ortiz (1992). An important feature of the present method is the direct identification of the active slip systems which, in our method, is calculated directly based on the current state of the crystal and the imposed incremental strain. The classical method used in many of authors relies on energy minimization and an iterative algorithm. It is important to note that in rate-dependent plasticity, there is no ambiguity as how to find all the active slip systems and the corresponding shear rates. However, in the rate-independent plasticity, there are inherently multiple possible sets of active slip systems whose identification requires additional assumptions; see Havner (1994) for a comprehensive account.

Nemat-Nasser et al. (1998a,b) use the results of a large number of experiments reported by Nemat-Nasser and Isaacs (1997) and Nemat-Nasser and Li (1998) for tantalum and copper, respectively, over broad ranges of strain rates and temperatures, to develop physics-based and experimentally-supported rate- and temperature-dependent constitutive models for slip rates in tantalum (with 48 potential slip systems) and copper (with 12 potential slip systems) crystals, calculating directly and unambiguously the slip rates of all active slip systems (up to 24 for tantalum and 8 for copper). Here, we implement this model for copper as a stand-alone single crystal or as a grain embedded in a polycrystalline matrix, including lattice elastic anisotropy. We also develop a complete algorithm for incremental calculation of stress, lattice orientation, temperature, and other necessary internal variables for applications to problems involving finite strains and rotations. In

summary, the present method has the following important features: (a) It uses experimen-tally-supported physics-based constitutive models for the slip rates; (b) It uses the explicit fully consistent plastic predictor–elastic corrector method; (c) It applies to fully aniso-tropic crystal elasticity and plasticity for finite deformations; and (d) It directly identifies all active slip systems and accurately produces their rates.

The flexibility and widespread availability of commercial finite element solvers has enabled researchers to develop material models and easily implement them in such codes without dealing with dynamics of any specific engineering problem. The integration of the equation of motion and satisfying boundary conditions are done by explicit finite element codes independently of the material constitutive routines. Therefore, in what follows we have considered that the final objective is to prepare a material subroutine for large-scale computations. In summary, we assume that the state of stress, the values of a specified set of internal (history) variables and the increment of strain for a given time interval are given and the stress state and the values of the internal variables at the end of this interval are required. However, unless explicitly specified, the examples area solved independently of any particular computational code. In the last part of the paper, several examples are solved with the help of LS-DYNA (Hallquist, 1998) for illustration. In these examples, zero traction boundary conditions are imposed and implemented by the finite element code. In short, when all of boundary conditions are of the deformation type, the machin-ery of a finite element solver is not required. In cases where a traction boundary condition is prescribed, the enforcement of this boundary condition is relegated to the finite element solver. The fortran subroutine is written such that it seamlessly integrates into the LS-DYNA finite element code.

2. Kinematics

For finite-deformation calculations, most finite element codes present the deformation increment during a time step at each integration point to the material constitutive routine. This increment is expressed in the material element coordinate system (MECS) rotating with the material element. For example, LS-DYNA uses the Hughes–Winget approxima-tion $\widehat{\mathbf{D}}^{\mathrm{HW}}$(Hughes and Winget, 1980). Assume that an estimate of $\widehat{\mathbf{D}}$, the deformation rate tensor in MECS (indicated with caret), is given to the constitutive subroutine. The objec-tive stress rate, in the same coordinate system, can be calculated from

$$\dot{\hat{\boldsymbol{\tau}}} = \widehat{\mathcal{L}} : (\widehat{\mathbf{D}} - \widehat{\mathbf{D}}^{\mathrm{p}}), \tag{1}$$

where $\widehat{\mathbf{D}}^{\mathrm{p}}$ is the plastic part of the deformation rate, $\widehat{L}$ is the elastic modulus tensor in MECS, and $\dot{\hat{\boldsymbol{\tau}}}$ is the time derivative of the Kirchhoff stress. Note that $\hat{\boldsymbol{\tau}} = J\hat{\boldsymbol{\sigma}} = \rho_0\hat{\boldsymbol{\sigma}}/\rho$ where J is the Jacobian of the deformation and $\hat{\sigma}$ is the Cauchy stress tensor. However, the elasticity tensor has to be calculated in the MECS which is different than the crystal-lographic axes coordinate system (CACS). The relation between MECS and CACS changes as the plastic deformation rotates the material with respect to the lattice. To ad-dress this and other related issues effectively, we write all equations and quantities in CACS. Quantities expressed in CACS are indicated with a tilde. In this convention the components of the elastic modulus tensor are simple and do not need to be adjusted with lattice rotation which is an important issue in finite deformations and rotations. Denote with $\mathbf{R}^{**T}$ the tensor that rotates the MECS unit triad, $\mathbf{e}_i$, into the CACS unit triad, $\mathbf{a}_i$:

$$\mathbf{a}_i = \mathbf{R}^{**T}\mathbf{e}_i = \left(\sum_{j=1}^{3}\mathbf{a}_j \otimes \mathbf{e}_j\right)\mathbf{e}_i = \left(\sum_{k,j=1}^{3}(\mathbf{a}_j \cdot \mathbf{e}_k)\mathbf{e}_k \otimes \mathbf{e}_j\right)\mathbf{e}_i. \tag{2}$$

The notation $\mathbf{R}^{**T}$ is chosen for compatibility with Nemat-Nasser (2004) which uses $\mathbf{R}^{**}$ to denote the rotation of the material through the crystal lattice due to the plastic deformation, based on the elasto-plastic decomposition $\mathbf{F} = \mathbf{F}^*\mathbf{F}^p = \mathbf{F}^*\mathbf{R}^{**}\mathbf{U}^p = \mathbf{V}^e\mathbf{R}^*\mathbf{R}^{**}\mathbf{U}^p$, following Lee (1969) and Willis (1969), as applied by Rice (1971) to single crystals. Note that we have exploited the indeterminacy in the two rotation tensors and used $\mathbf{R}^{**T}(t = 0)$ tensor for the initial rotation from MECS to CACS. The deformation rate in CACS is

$$\widetilde{\mathbf{D}} = \mathbf{R}^{**}\widehat{\mathbf{D}}\mathbf{R}^{**T}. \tag{3}$$

The rotation tensor is updated at the end of each time step. It is the integral of the plastic spin, or approximately,

$$\mathbf{R}^{**T}(t + \Delta t) = (1 + \widetilde{\mathbf{W}}^p\Delta t)\mathbf{R}^{**T}(t), \tag{4}$$

where the plastic spin is calculated from plastic slips, γ^α,

$$\widetilde{\mathbf{W}}^p = \sum\dot{\gamma}^\alpha\tilde{\mathbf{r}}_0^\alpha = \sum\dot{\gamma}^\alpha\frac{1}{2}(\tilde{\mathbf{s}}_0^\alpha \otimes \tilde{\mathbf{n}}_0^\alpha - \tilde{\mathbf{n}}_0^\alpha \otimes \tilde{\mathbf{s}}_0^\alpha). \tag{5}$$

The summation is over all possible slip systems. Note that, once $\widetilde{\mathbf{D}}^p = \sum\dot{\gamma}^\alpha\tilde{\mathbf{p}}_0^\alpha = \sum\dot{\gamma}^\alpha\frac{1}{2}(\tilde{\mathbf{s}}_0^\alpha \otimes \tilde{\mathbf{n}}_0^\alpha + \tilde{\mathbf{n}}_0^\alpha \otimes \tilde{\mathbf{s}}_0^\alpha)$, is established based on the constitutive relation, $\widetilde{\mathbf{W}}^p$ is uniquely determined. This is an important fact that is often neglected or misunderstood. A thorough discussion with supporting evidence and mathematical analysis can be found in Nemat-Nasser (2004). Eq. (4) is suitable for small time steps. Since in explicit finite element integration schemes, the time steps are provided by the code and generally are very small, this approximation is quite acceptable. However, when the time step becomes large, one may use an exact updating formula; for a detailed discussion of integration schemes with spin, see Nemat-Nasser (2004, Chapter 5). The crystallographic unit vectors in (5), represented in CACS, are constant:

$$\dot{\tilde{\mathbf{s}}}_0^\alpha = \dot{\tilde{\mathbf{n}}}_0^\alpha = 0. \tag{6}$$

3. Stress rate

The material subroutine has to return the updated stress tensor in MECS to the finite element solver. We calculate all the quantities in the CACS. The change of coordinate system is implemented at the end of the subroutine

$$\hat{\boldsymbol{\tau}} = \mathbf{R}^{**T}\widetilde{\mathbf{S}}^p\mathbf{R}^{**}, \tag{7}$$

where $\widetilde{\mathbf{S}}^p$ is the second Piola–Kirchhoff stress tensor in CACS. The rate of this stress measure is simply

$$\dot{\widetilde{\mathbf{S}}}^p = \widetilde{\boldsymbol{\mathcal{L}}} : (\widetilde{\mathbf{D}} - \sum\dot{\gamma}^\alpha\tilde{\mathbf{p}}_0^\alpha), \tag{8}$$

where the plastic rate of deformation is

$$\widetilde{\mathbf{D}}^{\mathrm{P}} = \sum \dot{\gamma}^{\alpha} \tilde{\mathbf{p}}_0^{\alpha} = \sum \dot{\gamma}^{\alpha} \frac{1}{2} (\tilde{\mathbf{s}}_0^{\alpha} \otimes \tilde{\mathbf{n}}_0^{\alpha} + \tilde{\mathbf{n}}_0^{\alpha} \otimes \tilde{\mathbf{s}}_0^{\alpha}). \tag{9}$$

The summation here is over all possible slip systems. The resolved shear stress on each slip system is

$$\tau^{\alpha} = \widetilde{\mathbf{S}}^{\mathrm{P}} : \tilde{\mathbf{p}}_0^{\alpha}. \tag{10}$$

The rate of this stress is

$$\dot{\tau}^{\alpha} = \dot{\widetilde{\mathbf{S}}}^{\mathrm{P}} : \tilde{\mathbf{p}}_0^{\alpha}. \tag{11}$$

Therefore we can write

$$\frac{1}{2\mu} \dot{\tau}^{\alpha} + \sum H^{\alpha\beta} \dot{\gamma}^{\beta} = d^{\alpha}, \tag{12}$$

where

$$H^{\alpha\beta} = \tilde{\mathbf{p}}_0^{\alpha} : \widetilde{\mathcal{L}}^n : \tilde{\mathbf{p}}_0^{\beta}, \tag{13}$$

$$d^{\alpha} = \tilde{\mathbf{p}}_0^{\alpha} : \widetilde{\mathcal{L}}^n : \widetilde{\mathbf{D}}, \tag{14}$$

$$\widetilde{\mathcal{L}}^n = \frac{1}{2\mu} \widetilde{\mathcal{L}}. \tag{15}$$

Here, μ is a normalizing modulus that coincides with the shear modulus in the isotropic case. Note that because of the interdependency of the slip systems $\tilde{\mathbf{p}}_0^{\alpha}$, only five of these equations for the rate of resolved shear stresses are linearly independent. The tensor $\widetilde{\mathcal{L}}^n$ has a simple form for cubic materials. After subtracting bulk modulus tensor, which can easily be dealt with independently, we can work with the deviatoric stress and strain rate tensors only. For cubic materials $\widetilde{\mathcal{L}}^n$ has the non-zero components:

$$\widetilde{\mathcal{L}}^n_{1111} = 2a/3, \quad \widetilde{\mathcal{L}}^n_{1122} = -a/3, \quad \widetilde{\mathcal{L}}^n_{1212} = 1/2, \tag{16}$$

and others that can be deduced based on cubic symmetry (Wikström and Nygård, 2002). Therefore, for any two symmetric and deviatoric tensors

$$\mathbf{c} : \widetilde{\mathcal{L}}^n : \mathbf{d} = a(c_{11}d_{11} + c_{22}d_{22} + c_{33}d_{33}) + 2(c_{12}d_{12} + c_{23}d_{23} + c_{31}d_{31}). \tag{17}$$

The parameter a is the anisotropy parameter and for copper is around 0.312. For isotropic materials it is equal to 1. It can be calculated form simple measurements along the crystallographic axes:

$$a = \frac{C_{11} - C_{12}}{2C_{44}}. \tag{18}$$

4. Integration schemes

Here we discuss the algorithms that are needed to integrate Eq. (12) for the plastic slip rates. We use two separate approaches based on whether the plastic part or the elastic part of the deformation is dominant. For the latter, we use an explicit forward-gradient method. When the plastic deformation is dominant we use a plastic predictor–elastic corrector method, following Nemat-Nasser and Okinaka (1996). However, note that since the rank of the matrix $H^{\alpha\beta}$ is only 5, when there are more than 5 active slip systems, we need

auxiliary conditions to find the plastic strain rates. These are selected from the interdependency relations of the resolved shear stresses and in general are written as

$$\sum M_{i\alpha}\tau^{\alpha} = 0. \tag{19}$$

There are exactly $N - 5$ independent such equations where N is the number of possible slip systems. For details of these interdependency relations see Nemat-Nasser and Okinaka (1996) or Nemat-Nasser (2004, Chapter 6). Written in an incremental form and along with (12), these will provide all necessary equations to directly calculate all the slip rates without any ambiguity. When there are more than 5 active slip systems or in fully-developed plastic flow, we use this expanded set of equations. Otherwise, we consider that the material in a transition regime and solve (12) without extra auxiliary equations, as they are no longer necessary. Finally, when the elastic contribution is relatively significant (which can only occur over a very small increment), we use an Euler forward-gradient algorithm with smaller time steps.

The algorithm starts in the rapidly-changing regime. In this regime, a slip system is considered active when its slip rate is greater than 0.1% of the applied effective rate of deformation $((2/3)\mathbf{D}':\mathbf{D}')^{1/2}$. When the number of active slip systems is between 1 and 5, the routine uses the transition regime algorithm. If the number of active slip systems is 6 or 8, the routine uses the fully-developed plastic algorithm. Sudden changes in the deformation state of the crystal (induced by sudden changes in the loading regime) will reset the method to the rapidly-changing algorithm for a finite number of steps (5 in most cases) before reevaluation. These changes include the addition of new active slip systems and significant changes in the slip rates. We have found out that when the change in the slip rates is more than 30% of the current value, we need to use the rapidly-changing algorithm to ensure stable calculations. This ratio is very large and can be adjusted to lower values if the solution lacks numerical stability.

4.1. Transition regime

The plastic predictor assumption is that the stress-rate term in (12) is very small and negligible, due to the fact that the magnitude of the shear modulus is much larger than the stress components. If the rate of the resolved shear stress is large enough, then one has to switch to forward-gradient method. Otherwise, one can start by solving the approximate linear equations:

$$\sum H^{\alpha\beta}\dot{\gamma}_{A}^{\beta} = d^{\alpha} \tag{20}$$

for the first approximation of the slip rates, $\dot{\gamma}_{A}^{\beta}$. To find the elastically-corrected value of the slip rates, integrate both (12) and (20) in time to obtain

$$\frac{1}{2\mu}\Delta\tau^{\alpha} + \sum H^{\alpha\beta}\Delta\gamma^{\beta} = d^{\alpha}\Delta t, \tag{21}$$

$$\sum H^{\alpha\beta}\Delta\gamma_{A}^{\beta} = d^{\alpha}\Delta t. \tag{22}$$

Subtraction gives

$$\sum H^{\alpha\beta}\gamma_{er}^{\beta} = \frac{\Delta\tau_{A}^{\alpha} - \tau_{er}^{\alpha}}{2\mu}, \tag{23}$$

where

$$\gamma_{\mathrm{er}}^{\alpha} = \Delta\gamma_A^{\alpha} - \Delta\gamma^{\alpha}, \tag{24}$$

$$\tau_{\mathrm{er}}^{\alpha} = \Delta\tau_A^{\alpha} - \Delta\tau^{\alpha}, \tag{25}$$

$$\Delta\tau_A^{\alpha} = F^{\alpha}(\dot{\gamma}_A^{\alpha}, \gamma_A^{\beta}, T_A) - \tau^{\alpha}(t_0), \tag{26}$$

$$\gamma_A^{\alpha} = \gamma^{\alpha}(t_0) + \Delta\gamma_A^{\alpha} = \gamma^{\alpha}(t_0) + \mathrm{sgn}(\dot{\gamma}_A^{\alpha})(\theta\dot{\gamma}^{\alpha}(t_0) + (1-\theta)\dot{\gamma}_A^{\alpha})\Delta t, \tag{27}$$

$$T_A = T(t_0) + \Delta T_A = T(t_0) + \eta \sum \tau^{\alpha}\Delta\gamma_A^{\alpha}. \tag{28}$$

Here, θ is an integration parameter between 0 and 1, and $\eta = \bar{\eta}/\rho c$, where $\bar{\eta}$ is the ratio of inelastic mechanical work that turns into heat (very close to 1 for most metals), ρ is the mass density and c is the heat capacity at constant volume. The yield conditions on the αth slip system is $\tau^a = F^{\alpha}(\dot{\gamma}^{\alpha}, \gamma^{\beta}, T)$ which stands for $F^{\alpha}(\dot{\gamma}^{\alpha}, \gamma^1, \gamma^2, \ldots, \gamma^N, T)$. The increments in (27) and (28) are of the order of the time step. In general this equation can be solved using the expressions

$$\gamma_{\mathrm{er}}^{\alpha} = (1-\theta)\dot{\gamma}_{\mathrm{er}}^{\alpha}\Delta t, \tag{29}$$

$$T_{\mathrm{er}} = (1-\theta)\eta \sum \tau^{\beta}\dot{\gamma}_{\mathrm{er}}^{\beta}\Delta t, \tag{30}$$

$$\tau_{\mathrm{er}}^{\alpha} = \left.\frac{\partial F^{\alpha}}{\partial\dot{\gamma}^{\alpha}}\right|_{\dot{\gamma}_A^{\alpha}}\dot{\gamma}_{\mathrm{er}}^{\alpha} + \sum \left.\frac{\partial F^{\alpha}}{\partial\gamma^{\beta}}\right|_{\gamma_A^{\beta}}\gamma_{\mathrm{er}}^{\beta} + \left.\frac{\partial F^{\alpha}}{\partial T}\right|_{T_A}T_{\mathrm{er}}. \tag{31}$$

After rewriting (23) in terms of error slip rates $\dot{\gamma}_{\mathrm{er}}^{\alpha}$ and eliminating $\gamma_{\mathrm{er}}^{\alpha}$, T_{er}, and $\tau_{\mathrm{er}}^{\alpha}$ using (29)–(31), we arrive at a new set of linear equations that can be solved for the error terms $\dot{\gamma}_{\mathrm{er}}^{\alpha}$. However, observe that (29) and (30) (the decrement in resolved shear stress error due to the error in the plastic strains and temperature) are of the order of time step multiplied by the $\dot{\gamma}_{\mathrm{er}}^{\alpha}$ (the decrement due to the error in the slip rates). The coefficients in (31) have to be estimated as well but in the cases studied in this paper the first term is dominant. This gives the following linear equation for the error terms:

$$\sum G^{\alpha\beta}\dot{\gamma}_{\mathrm{er}}^{\beta} = \frac{\Delta\tau_A^{\alpha}}{2\mu\Delta t}, \tag{32}$$

$$G^{\alpha\beta} = (1-\theta)H^{\alpha\beta} + \frac{1}{2\mu\Delta t}\left.\frac{\partial F^{\alpha}}{\partial\dot{\gamma}^{\alpha}}\right|_{\dot{\gamma}_A^{\alpha}}. \tag{33}$$

It must be noted here that if the second and third terms in (31) are not negligible, then (33) can be simply modified to include those terms as well. For further detail see Nemat-Nasser et al. (1998a).

4.2. Fully-developed plastic regime

When the number of active slip systems is greater than 5, Eq. (20) for predictor and (32) are not enough to solve for all non-zero slip rates. We utilize the auxiliary conditions in (19). To use with (23), we write (19) in incremental form

$$\sum M_{i\alpha}\Delta\tau_A^{\alpha} = 0. \tag{34}$$

Linearization gives the approximate formula

$$\sum M_{i\alpha} \left(\frac{\partial F^\alpha}{\partial \dot{\gamma}^\alpha} \bigg|_{\dot{\gamma}^\alpha(t_0)} \Delta \dot{\gamma}^\alpha_A + \sum \frac{\partial F^\alpha}{\partial \gamma^\beta} \bigg|_{\gamma^\alpha(t_0)} \Delta \gamma^\beta_A + \frac{\partial F^\alpha}{\partial T} \bigg|_{T(t_0)} \Delta T_A \right) = 0. \tag{35}$$

This can be rearranged using 26, 27, 27 in the general form:

$$\sum C_{i\alpha} \dot{\gamma}^\alpha_A = b_i, \tag{36}$$

which can be combined with (20) without further manipulation. In many cases, these coefficients can easily be calculated directly and explicitly; Nemat-Nasser and Okinaka (1996) have calculated them for the power-law constitutive equation, and Nemat-Nasser et al. (1998a) for the present physics-based model. The new matrix consisting of $H^{\alpha\beta}$ and $C_{i\beta}$ is inverted as a whole to give the plastic predictor values $\dot{\gamma}^\alpha_A$. For the elastic correction, write

$$\sum M_{i\alpha} \Delta \tau^\alpha = 0, \tag{37}$$

$$\sum M_{i\alpha} \left(\frac{\partial F^\alpha}{\partial \dot{\gamma}^\alpha} \bigg|_{\dot{\gamma}^\alpha(t_0)} (\Delta \dot{\gamma}^\alpha_A - \dot{\gamma}^\alpha_{er}) + \sum \frac{\partial F^\alpha}{\partial \gamma^\beta} \bigg|_{\gamma^\alpha(t_0)} (\Delta \gamma^\beta_A - \gamma^\alpha_{er}) \right.$$
$$\left. + \frac{\partial F^\alpha}{\partial T} \bigg|_{T(t_0)} (\Delta T_A - T_{er}) \right) = 0. \tag{38}$$

This gives

$$\sum C_{i\alpha} (\dot{\gamma}^\alpha_A - \dot{\gamma}^\alpha_{er}) = b_i. \tag{39}$$

Subtraction from (36) gives

$$\sum C_{i\alpha} \dot{\gamma}^\alpha_{er} = 0. \tag{40}$$

Although one can achieve a better approximation than (40) through linearization of (37) around $\dot{\gamma}^\alpha_A$, but the fact that the order of magnitude of the error terms in (40) is much smaller than $\dot{\gamma}^\alpha_A$ makes this unnecessary. Eq. (40) supplement (32) to give the error values for all active slip systems even when the number is larger than 5.

4.3. Rapidly-changing regime

When the elastic deformation is dominant, the plastic predictor approximation involves significant errors. In this case, we use small time steps and solve (12) iteratively, assuming the slip rates are the same as the previous time step initially and calculate an approximate rate of the resolved shear stress from

$$\dot{\tau}^\alpha = 2\mu (d^\alpha - \sum H^{\alpha\beta} \dot{\gamma}^\beta(t_0)). \tag{41}$$

We update the resolved shear stresses by integration of the left-hand side of (41), and subsequently the slip rates on all slip systems are calculated through

$$\dot{\gamma}^\alpha = (F^\alpha)^{-1} (\tau^\alpha, \gamma^\beta, T). \tag{42}$$

If the difference between the new slip rates and those used in (41) from the previous time step is appreciable, this step is repeated until convergence is achieved. Although the amount of the calculations at each step seems to be far less than the previous two regimes,

the iteration has to be performed many times, whereas there are no iterations required in the fully-developed plastic or the transition algorithms.

4.4. Stress tensor update

At the end of any of the above methods, we update the resolved shear stresses. We select five independent equations from those available in (10) and solve them for the components of the stress tensor. Finally the lattice orientation is updated through (4) and using (7) to calculate the stress tensor in material element coordinate system finishes the required steps in the constitutive algorithm.

5. Physics-based material model

A dislocations-based model of plasticity that includes both temperature- and strain-rate effects has been developed for fcc metals by Nemat-Nasser and Li (1998), heavily drawing from a large set of experimental data on OFHC copper over broad ranges of strain rates and temperatures. The model has also been detailed by Nemat-Nasser (2004) in a recent book; a brief account has also been included in a more recent paper by Nemat-Nasser et al. (2006). For completeness, however, we outline the basic results in this section.

We define the slip rate of a given slip system by the Orowan equation, $\dot{\gamma} = b\rho_m v$, where v is the average dislocation velocity, ρ_m is the density of the mobile dislocations producing the slip, and b is the magnitude of the Burgers vector. The average dislocation velocity is expressed in terms of the density of the short-range barriers that the dislocations must overcome in their motion, and their average activation energy, ΔG. For fcc and some hcp metals, the total dislocations that intersect the slip plane are the primary short-range barriers to the motion of the mobile dislocations lying on the slip plane. To estimate this average velocity, we divide the average spacing of the short-range barriers, l_s, by the sum of the average waiting time to cross the barrier, t_w, and the running time, t_r, to move between the barriers (Regazzoni et al., 1987), $v = l_s/(t_w + t_r)$. Here, we neglect t_r and set $t_w = \omega_0^{-1} \exp(\Delta G/kT)$, where ω_0 is the total attempt frequency (which depends on the dislocation core structure), T is the absolute temperature, and k is Boltzmann's constant. Combining the above expressions, we arrive at the following estimate for the slip rate:

$$\dot{\gamma} = \dot{\gamma}_0 \left(\frac{l'_s}{l'^2_m} \right) \exp(-\Delta G/kT), \tag{43}$$

$$l'_s = \frac{l_s}{l_0}, \tag{44}$$

$$l'_m = \frac{l_m}{l_0}, \tag{45}$$

where $\dot{\gamma}_0 = b\omega_0/l_0$ is a reference slip rate, l_0 is some convenient reference length corresponding to a reference strain rate, and $l_m = \rho_m^{-1/2}$ is the average spacing of the mobile dislocations. For fcc crystals, one may use the average spacing of the total dislocations at some reference state for l_0. In Eqs. (43)–(45), l_s and l_m are viewed as natural length scales that characterize the microstructure and dislocation activities, evolving with the temperature and deformation histories. They thus require evolutionary constitutive descriptions.

For a typical slip system, we use the following expression to define the activation energy of the dislocations associated with this slip system:

$$\Delta G = G_0 \left[1 - \left(\frac{\tau - \tau_a}{\hat{\tau}} \right)^p \right]^q, \tag{46}$$

$$\hat{\tau} = \frac{G_0}{b \lambda l} = \frac{\hat{\tau}_0}{l'}, \tag{47}$$

$$\hat{\tau}_0 = \frac{G_0}{b \lambda l_0}, \tag{48}$$

$$l' = \frac{l}{l_0}. \tag{49}$$

Here, τ is the resolved shear stress in the slip direction, τ_a (the stress due to the long-range barriers) is the resistance imposed on the moving dislocations by the elastic stress field of all dislocations and defects, G_0 is the total short-range barrier's energy, λ and $\hat{\tau}_0 = \frac{G_0}{b \lambda l_0}$, p, and q define the structure of the short-range barriers. In (47) and (49), l' is another normalized length scale that characterizes the distribution and structure of the short-range barriers. Eq. (46) has been obtained empirically by the Nemat-Nasser and co-workers, but it has a long history going back to Ono (1968) and Kocks et al. (1975). Ono suggests $0 < p \leqslant 1$ and $1 \leqslant q \leqslant 2$ for most energy barrier profiles. We have now extensive experimental data for many bcc, fcc, and hcp metals, all which support Ono's suggestion; see Tables 4.8.1 and 4.8.2, pp. 235 and 238 of Nemat-Nasser (2004). The parameter λ is absorbed in $\hat{\tau}_0$ which is established experimentally.

The resistance of the long-range barriers, τ_a, is referred to as the athermal component of the slip resistance. Being due to the elastic field of the dislocations and defects, its dependence on temperature is through the temperature dependence of the elastic moduli, especially the shear modulus, $\mu(T)$, and the temperature-history dependence of the microstructure, e.g., dislocation density. We set

$$\tau_a = \hat{g}(\rho_t, \ldots)\mu(T)/\mu_0, \tag{50}$$

$$l'_t = \frac{l_t}{l_0}, \tag{51}$$

where ρ_t is the average total dislocation density, the dots stand for parameters associated with other defects and impurities that help to create an elastic stress field, μ_0 is a reference value of the shear modulus, and $l_t = \rho_t^{-1/2}$ is another natural length scale that correspond to the average spacing of all dislocations. To simplify this expression, we use the effective plastic strain associated with all slip systems, γ_{eff}, which is a non-decreasing quantity, as our "loading parameter", and approximate (50) by

$$\tau_a = \tau_a^0 + \tau_a^{00} \gamma_{\text{eff}}^{n_1}, \tag{52}$$

viewing τ_a^0, τ_a^{00}, and n_1 as constitutive parameters to be fixed experimentally.

Eqs. (43)–(52) now define the slip rate in terms of the resolved shear stress, τ, temperature, T, and four normalized length parameters, l', l'_m, l'_s, and l'_t. These length scales directly relate to the physics of dislocation-induced plastic deformation of metals. Their evolution with deformation and temperature must be modeled based on experimental results and physical arguments. Expression (52) accounts approximately for the length scale l'_t. To obtain approximations for the other three length scales, note that the disloca-

tion density on a slip plane increases with continued plastic slip and decreases with increasing temperature, T. As a first approximation, we set

$$\frac{l'_s}{l'^2_m} \approx l' \approx \frac{1}{f(\gamma_{eff}, T)}, \tag{53}$$

where the function f must be increasing with γ_{eff}, and decreasing with T. It has been found by Nemat-Nasser and Li (1998) that the following approximation may be used for OFHC copper:

$$f(\gamma_{eff}, T) \approx 1 + a_0 \left(1 - \left(\frac{T}{T_m} \right)^2 \right) \gamma_{eff}^m, \tag{54}$$

where a_0 and m are constitutive parameters and T_m is the melting temperature.

6. Application: modeling the response of copper as a single crystal and a grain in a polycrystalline film

In this section we present the results of calculations on the constitutive behavior of single crystal copper in various loading condition. Two sets of material parameters for the physics-based constitutive models described in the previous section are used. The following values are the same for both cases, the bulk modulus $K = 140$ GPa, the shear modulus $\mu = 80$ GPa, the energy barrier parameters $p = 2/3$, $q = 2$, and $k/G_0 = 4.9 \times 10^{-5}$/K, the constant power for dislocation spacing evolution $m = 1/2$, the reference slip rate $\dot{\gamma}_0 = 2 \times 10^{10}$/s, the melting temperatures, $T_m = 1350$ K, and finally the parameter for temperature rise calculation due to the plastic work $\eta = 0.433$ K/J/m^3 equivalent to 100% of the inelastic mechanical work turning into heat. The last parameter is only used for high-rate cases where due to the short time scales involved the dissipated plastic work heats the material locally and adiabatically. In all cases the integration parameter is taken constant $\theta = 0.1$, and the material is considered to be initially at room temperature $T_0 = 296$ K. When the full elasticity tensor of copper with cubic symmetry is considered, the value of the anisotropy parameter is $a = 0.312$, where for elastically isotropic cases $a = 1$ is used. In the first set of calculations we used the following values for the remaining parameters $\tau_a^0 = 5$ MPa, $\tau_a^{00} = 70$ MPa, $n_1 = 0.5$, $\hat{\tau}_0 = 130$ MPa, $a_0 = 1.8$. In comparison, to reproduce the experimental results reported in Hommel and Kraft (2001) these parameters are chosen based on the continuum values reported in Nemat-Nasser and Li (1998): $\tau_a^0 = 10$, $\tau_a^{00} = 220$ MPa, $n_1 = 0.3$, $\hat{\tau}_0 = 46$ MPa, $a_0 = 20$. Also to be consistent with Hommel and Kraft (2001) experiments, we used a constant strain rate $D_{11} = 10^{-7}$/s. The strain rate history for other cases was prescribed as $((2/3)\mathbf{D}':\mathbf{D}')^{1/2} = Af(t)$, where A is a dimensionless constant and in most case equal to 1, and $f(t)$ is a function of time shown in Fig. 1. This function includes periods of different rates as well as unloading and reverse-loading portions.

The results in Fig. 2 show the stress components when the deformation rate tensor orientation is chosen such that initially only one slip system can be active: $\tilde{\mathbf{s}}_0^1 \otimes \tilde{\mathbf{n}}_0^1 = (1/\sqrt{6})(\mathbf{a}_1 - \mathbf{a}_2) \otimes (\mathbf{a}_1 + \mathbf{a}_2 + \mathbf{a}_3)$. The deformation rate tensor is given by $(A = 1/\sqrt{3})$
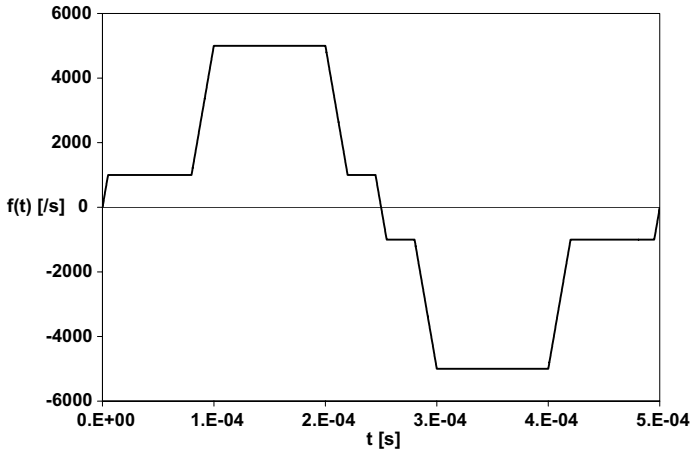
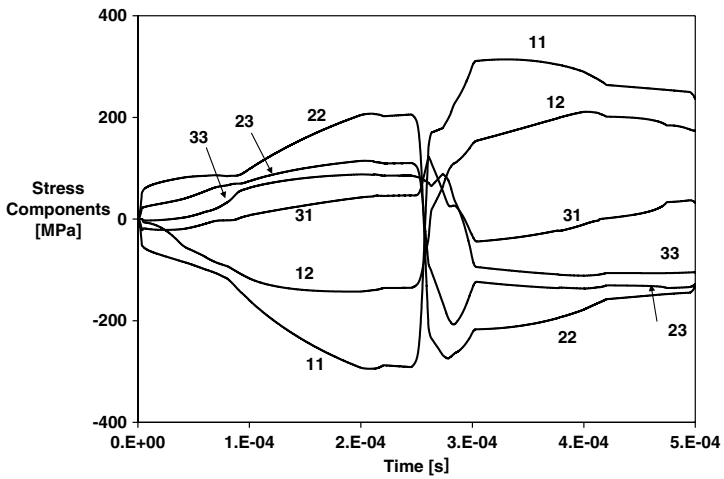Fig. 1. Strain rate history as a function of time for variable-rate calculations.

Fig. 2. The components of the Kirchhoff stress tensor $\hat{\boldsymbol{\tau}}$ in MECS for the loading described in (55) and (56) that initially activates a single slip system.

$$\widehat{\mathbf{D}} = f(t) \begin{bmatrix} -1/2 & 0 & 0 \\ 0 & 1/2 & 0 \\ 0 & 0 & 0 \end{bmatrix}. \tag{55}$$

And the transformation tensor is initially given by

$$\mathbf{R}^{**T}(t=0) = \begin{bmatrix} 0.90825 & -0.09175 & 0.40825 \\ -0.09175 & 0.90825 & 0.40825 \\ -0.40825 & -0.40825 & 0.8165 \end{bmatrix}. \tag{56}$$
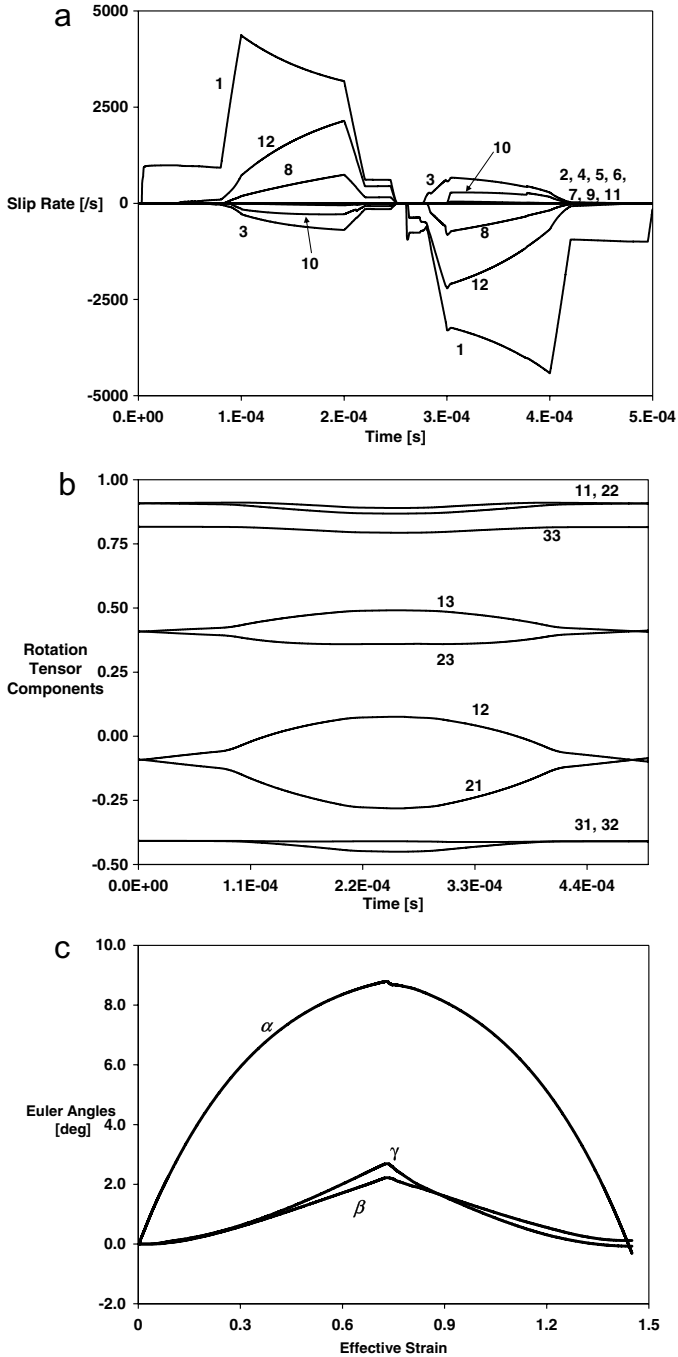
Fig. 3. Results of the constitutive algorithm for the loading described in (55) and (56). (a) The slip rates on all 12 possible slip systems. Note that initially only one system is active and other systems (up to six in this case) become active one at a time. (b) The components of the rotation tensor $\mathbf{R}^{**T}$ as a function of time. (c) The changes in Euler angles of the rotation matrix.

Note that the columns of (56) are the vector components of the crystallographic unit triad in MECS. Fig. 3 shows the slip rates of all 12 slip systems, the components of the transformation tensor $\mathbf{R}^{**T}(t)$ as the deformation progresses, and the change in Euler angles (in °) of this rotation tensor as a function of the effective strain. Note the significant reorientation of the lattice with respect to the material element. The number of active slip systems start with 1 but increases by steps of 1–6.

The effect of the loading direction with respect to the crystallographic axes is shown in Fig. 4. Here, the effective stress $\tau = ((3/2)\hat{\tau}' : \hat{\tau}')^{1/2} = ((3/2)\tilde{\mathbf{S}}^{P'} : \tilde{\mathbf{S}}^{P'})^{1/2}$ is plotted versus the effective strain $\gamma(t) = \int_0^t ((2/3)\mathbf{D}'(\xi) : \mathbf{D}'(\xi))^{1/2}\mathrm{d}\xi$. The loading is applied along the material X-axis which has the crystallographic indices shown in Fig. 4 ($A = 1$):
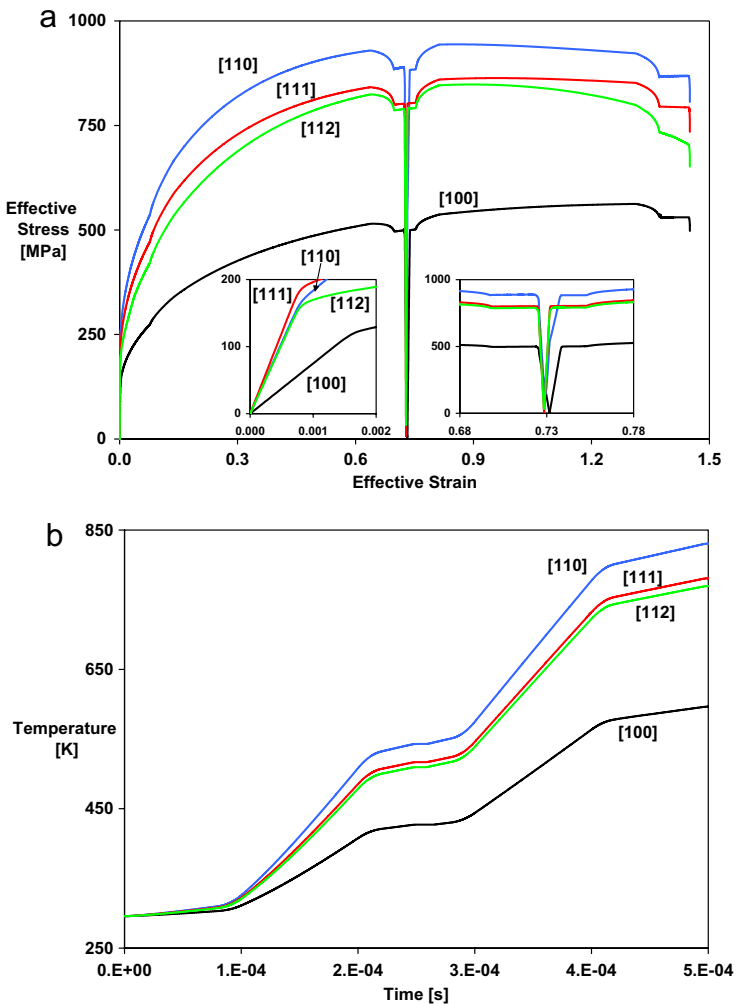

Fig. 4. Comparison among loadings along various crystallographic axes. The elements are loaded as shown in (57) with material X-axis along the crystallographic axis shown in the graph. (a) The effective stress versus the effective strain. (b) The temperature increase with time.

$$\widehat{\mathbf{D}} = f(t) \begin{bmatrix} 1 & 0 & 0 \\ 0 & -1/2 & 0 \\ 0 & 0 & -1/2 \end{bmatrix}. \tag{57}$$

The $\mathbf{R}^{**T}(t=0)$ can be easily calculated for all these cases. Also shown in Fig. 4 is the temperature history for these four cases.

Although the effect of the cubic symmetry of the lattice on the plastic response of the crystal is clear from Fig. 4, we show here that the elastic anisotropy also affects the mechanics of the deformation, especially during elastic loading and unloading. To observe this, see Fig. 5, where the effective stress is plotted versus effective strain when the crystal is loaded along [1 0 0] axis according to Eq. (57). The difference when the crystal is considered elastically isotropic and when it has the physical cubic symmetry is demonstrated. When the loading is not proportional, that is when the principal axes of the deformation change through the course of the deformation, this difference becomes more pronounced.

The correct elastic correction based on (32), (33) and (40) is equally important in these situations. When the elastic share of the deformation is significant, these corrections change the calculated response. Moreover the error due to the omission of these corrections can be accumulated. The examples shown in Fig. 6 demonstrate this effect. Here, the axial stress versus axial strain and effective stress versus effective strain are plotted for two different kinds of loading.

When the elastic and/or plastic response of a material is anisotropic, the choice of appropriate boundary conditions becomes important. We have used displacement boundary conditions for all the examples in this paper up to this point. The stress components shown in Fig. 7 are also for such boundary conditions. Here, the deformation rate tensor according to (57) is applied along two different axes, namely [1 1 0] and [1 1 1]. Although the applied deformation in both cases is symmetric around the material X-axis, the stress
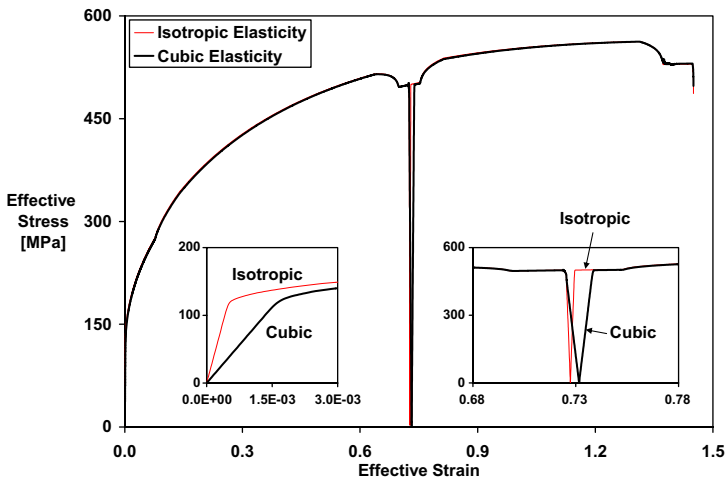

Fig. 5. Comparison between the responses of a single crystal when the elastic modulus tensor is considered isotropic versus when it has cubic symmetry. The plastic flow is not affected much. However the elastic loading and unloading are significantly changed. In this example the FCC crystal is loaded along its [1 0 0] axis according to Eq. (57).
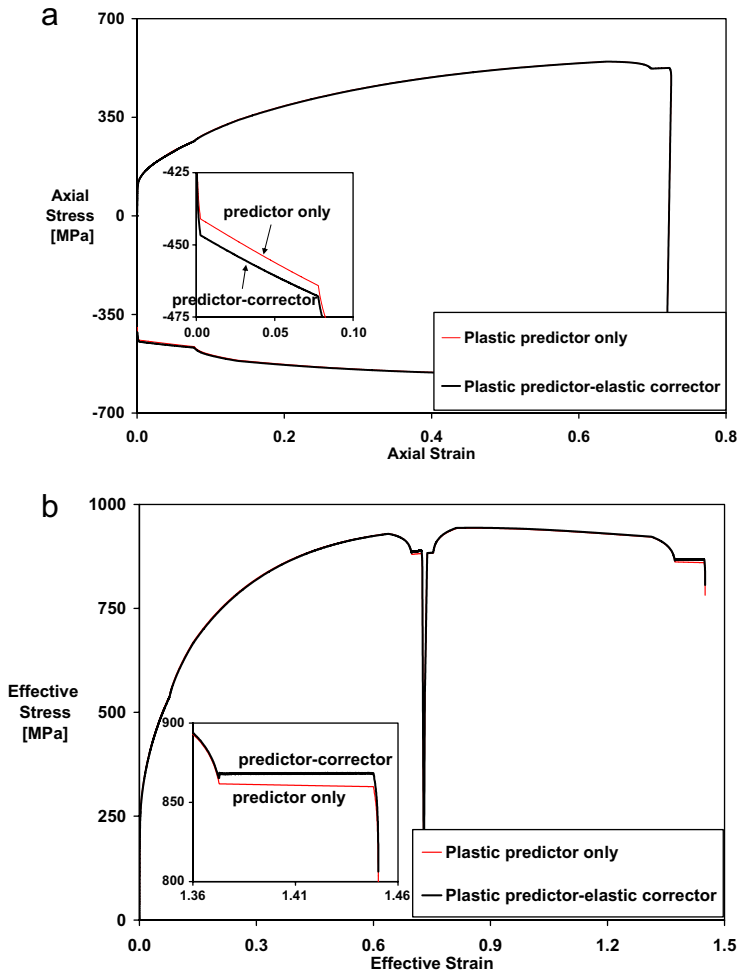
Fig. 6. Effect of elastic correction on the calculated response. (a) The axial (11) stress component versus axial strain. The cumulative effect is noticeable at the end of the calculation. In this case the crystal is loaded along its [1 1 2] axis according to Eq. (57). (b) Similarly for the effective stress versus effective strain. In this case the crystal is loaded along its [1 1 1] axis.

tensor is significantly different. In [1 1 0] loading, though for most of the course of the deformation there are 8 active slip systems, the 22 component of stress is non-zero only for a short time during the unloading and reverse loading. On the other hand in [1 1 1] loading, though only a maximum of 6 slip systems become active, the stress tensor also has symmetry around the X-axis. For more asymmetric loading such as [1 1 2], some of the shear components of the stress tensor become non-zero as well, in this case the 31 component. In other words, except in special cases, symmetry of loading in the stress space is not compatible with it in deformation space.

As a further example and to demonstrate the boundary condition effect, we tried to reproduce the experimental results of Hommel and Kraft (2001) on thin copper films.
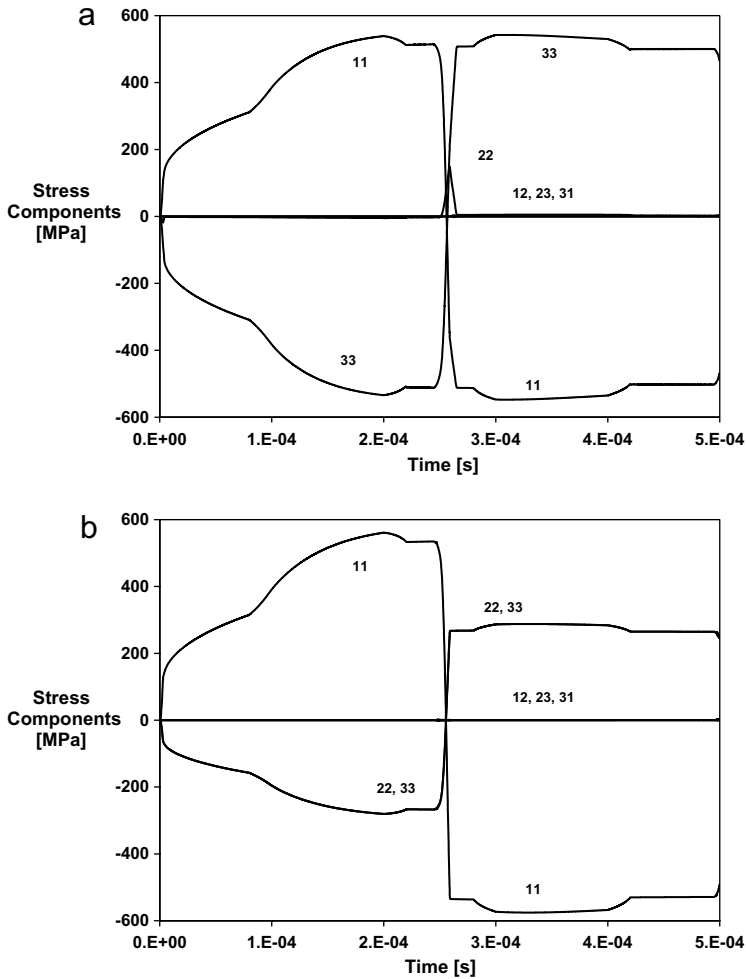
Fig. 7. Stress components for deformation loading along (a) [1 1 0] and (b) [1 1 1] axes according to Eq. (57). Note that in (b) the stress tensor is fully symmetric around the material *X*-axis, unlike (a).

Following Nemat-Nasser et al. (2006), the material parameters that were experimentally established by Nemat-Nasser and Li (1998) were used. Unlike Nemat-Nasser et al. (2006), where isotropic elasticity with an adjusted axial Young's modulus is used for simulation, here we used the physical elasticity modulus for copper with cubic symmetry. The slope of the elastic segment of the curve is reproduced automatically and without further adjustment. Moreover the boundary conditions are selected such that to simulate the conditions of the experiment as closely as possible. To this end, we applied traction free boundary conditions on the free surfaces of the film, while applying zero displacement in the plane of the film and prescribed motion along the loading direction with $D_{11} = 10^{-7}$/s. The only difference in material parameters between this example and other examples in this work are $\tau_a^0 = 10, \tau_a^{00} = 220$ MPa, $n_1 = 0.3, \hat{\tau}_0 = 46$ MPa, $a_0 = 20$, which are more appropriate for annealed copper. The results agree very well with the experimental
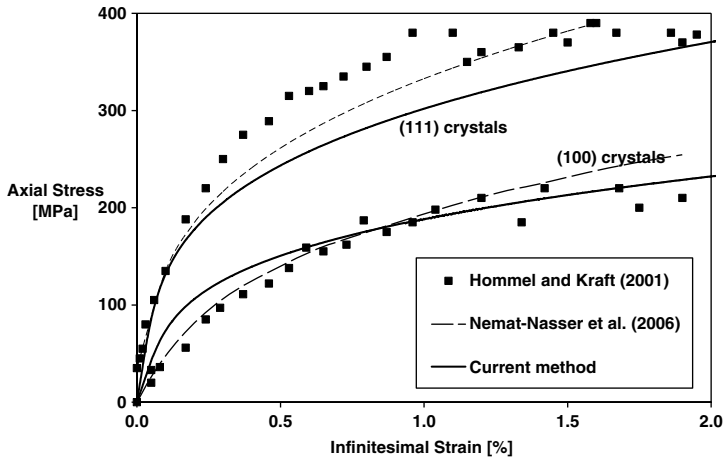
Fig. 8. Comparison between the experimental data from Hommel and Kraft (2001) and the method presented in Nemat-Nasser et al. (2006) and the current work. The (1 0 0) and (1 1 1) crystals are loaded along [0 0 1] and [$\bar{2}$1 1] axes, respectively. Since the sample is a film, of the two other boundary conditions, one is prescribed as zero displacement boundary while the other is a traction free surface.

data and are plotted in Fig. 8. These results are calculated using LS-DYNA with the user-defined material subroutine for plastic predictor–elastic corrector explicit integration scheme for crystal plasticity model mentioned previously. In addition to the elastic slope being automatically reproduced, the effect of boundary conditions is clearly seen in this example in comparison with the results of Nemat-Nasser et al. (2006). In the present calculations, the same material properties are used for both examples, including the elasticity tensor with cubic crystal symmetry and the athermal yield stress at zero strain. These quantities are adjusted in Nemat-Nasser et al. (2006) based on physical considerations. For example, the elasticity tensor used in this reference is isotropic and the shear modulus is adjusted for each crystal orientation. While for this special case with small deformations one can do such manual adjustment in the elasticity, this is not possible when finite rotations and deformations are involved with elastic anisotropy. Furthermore, the exact physical boundary conditions are used in the present calculations, while in the previous work an equivalent prescribed deformation is used for all cases.

7. Summary

A framework for numerical explicit integration of various constitutive models of crystal elasto-plasticity is developed and used. A physics-based material subroutine for FCC crystals is coded in FORTRAN and used independently or as a user subroutine for LS-DYNA. Various examples show the applicability and power of the proposed method. Some comparison with recent experimental results and numerical models are presented.

Acknowledgements

and a more direct evaluation of the active slip systems. This work was partially supported by ONR N00014-02-1-0666 to UC San Diego.

References

Bate, P., 1999. Modeling deformation microstructure with the crystal-plasticity finite element-method. Proc. Roy. Soc. London A 357, 1589–1601.

Beaudoin, A.J., Mathur, K.K., Dawson, P.R., Johnson, G.C., 1993. Three-dimensional deformation process simulation with explicit use of polycrystal plasticity models. Int. J. Plasticity 9, 833–860.

Bishop, J.F.W., Hill, R., 1951a. A theory of the plastic distortion of a polycrystalline aggregate under combined stresses. Phil. Mag. 42, 414–427.

Bishop, J.F.W., Hill, R., 1951b. A theoretical derivation of the plastic properties of a polycrystalline face centered metal. Phil. Mag. 42, 1298–1307.

Bronkhorst, C.A., Kaldindini, S.R., Anand, L., 1992. Polycrystalline plasticity and the evolution of crystallographic texture in FCC metals. Phil. Trans. Roy. Soc. London A 341, 443–477.

Cuitiño, A.M., Ortiz, M., 1992. Computational modelling of single crystals. Model. Simul. Mater. Sci. Eng. 1, 225–263.

Hallquist, J.O., 1998. LS-DYNA Theoretical Manual. LSTC, Livermore, CA.

Havner, K., 1994. Finite Plastic Deformation of Crystalline Solids. Cambridge University Press, Cambridge.

Hommel, M., Kraft, O., 2001. Deformation behavior of thin copper films on deformable substrates. Acta Mater. 49, 3935–3947.

Hughes, T.J.R., Winget, J., 1980. Finite rotation effects in numerical integration of rate-constitutive equations arising large-deformation analysis. Int. J. Numer. Meth. Eng. 15, 1862–1867.

Kaldindini, S.R., Bronkhorst, C.A., Anand, L., 1992. Crystallographic texture evolution in bulk deformation processing of FCC metals. J. Mech. Phys. Solids 40, 537–569.

Kocks, U.F., Argon, A.S., Ashby, M.F., 1975. Thermodynamics and kinetics of slip. Prog. Mater. Sci. 19, 1–271.

Kuchnicki, S.N., Cuitiño, A.M., Radovitzky, R.A., 2006. Efficient and robust constitutive integrators for single-crystal plasticity modeling. Int. J. Plasticity 22, 1988–2011.

Lee, E.H., 1969. Elastic–plastic deformation at finite strains. J. Appl. Mech. 36, 1–6.

Lin, T.H., 1957. Analysis of elastic and plastic strains of a face-centered cubic crystal. J. Mech. Phys. Solids 5, 143–149.

Lin, T.H., Ito, M., 1966. Theoretical plastic stress–strain relationship of a polycrystal and the comparison with the von Mises and the Tresca plasticity theories. Int. J. Eng. Sci. 4, 543–546.

McGinty, R.D., McDowell, D.L., 2006. A semi-implicit integration scheme for rate-independent finite crystal plasticity. Int. J. Plasticity 22, 996–1025.

Nemat-Nasser, S., 2004. Plasticity: A Treatise on the Finite Deformation of Heterogeneous Inelastic Materials. Cambridge University Press, Cambridge.

Nemat-Nasser, S., Isaacs, J., 1997. Direct measurement of isothermal flow stress of metals at elevated temperatures and high strain rates with application to Ta and Ta–W alloys. Acta Mater. 54, 907–919.

Nemat-Nasser, S., Li, S.Y., 1998. Flow stress of FCC polycrystals with application to OFHC Cu. Acta Mater. 46, 565–577.

Nemat-Nasser, S., Obata, M., 1986. Rate-dependent, finite elasto-plastic deformation of polycrystals. Proc. Roy. Soc. London A 407, 343–375.

Nemat-Nasser, S., Okinaka, T., 1996. A new computational approach to crystal plasticity: FCC single crystal. Mech. Mater. 24, 43–57.

Nemat-Nasser, S., Ni, L., Okinaka, T., 1998a. A constitutive model for FCC crystals with application to polycrystalline OFHC copper. Mech. Mater. 30, 325–341.

Nemat-Nasser, S., Okinaka, T., Ni, L., 1998b. A physically-based constitutive model for bcc crystals with application to polycrystal tantalum. J. Mech. Phys. Solids 46, 1009–1038.

Nemat-Nasser, S., Maximenko, A., Olevsky, E., 2006. Modeling the plastic response of thin metal membranes. J. Mech. Phys. Solids 54, 2474–2494.

Ono, K., 1968. Temperature dependence of dispersed barrier hardening. J. Appl. Phys. 39, 1803–1806.

Orowan, E., 1934. Zur Kristallplastiztät – I, II, III. Zeit. Phys. 89, 605–659.

Peirce, D., Asaro, R.J., Needleman, A., 1983. Material rate-dependence and localized deformation in crystalline solids. Acta Metall. 31, 1951–1976.

Polanyi, M., 1934. Über eine Art Gitterstörung, die eine Kristall plastisch machen konnte. Zeit. Phys. 89, 660–664.

Rashid, M.M., Nemat-Nasser, S., 1992. A constitutive algorithm for rate-dependent crystal plasticity. Comp. Meth. App. Mech. Eng 94, 201–228.

Regazzoni, G., Kocks, U.F., Follansbee, P.S., 1987. Dislocation kinetics at high strain rates. Acta Metall. 35, 2865–2875.

Rice, J., 1971. Inelastic constitutive relations for solids: an internal variable theory and its application to metal plasticity. J. Mech. Phys. Solids 19, 433–455.

Taylor, G.I., 1934. The mechanism of plastic deformation of crystals – I, II. Proc. Roy. Soc. London A 145, 362–387, 388–404.

Wikström, A., Nygård, M., 2002. Anisotropy and texture in thin copper films – an elasto-plastic analysis. Acta Mater. 50, 857–870.

Willis, J.R., 1969. Some constitutive equations applicable to problems of large dynamic plastic deformation. J. Mech. Phys. Solids 17, 359–369.